Biophysical Journal
Article

Biophysical Society

Quantitative Characterization of Metastability and Heterogeneity of Amyloid Aggregates

Timir Baran Sil,[1] Bankanidhi Sahoo,[1] Subhas Chandra Bera,[1] and Kanchan Garai[1,*]
[1]Tata Institute of Fundamental Research, Serilingampally, Hyderabad, India

ABSTRACT Amyloids are heterogeneous assemblies of extremely stable fibrillar aggregates of proteins. Although biological activities of the amyloids are dependent on its conformation, quantitative evaluation of heterogeneity of amyloids has been difficult. Here we use disaggregation of the amyloids of tetramethylrhodamine-labeled Aβ (TMR-Aβ) to characterize its stability and heterogeneity. Disaggregation of TMR-Aβ amyloids, monitored by fluorescence recovery of TMR, was negligible in native buffer even at low nanomolar concentrations but the kinetics increased exponentially with addition of denaturants such as urea or GdnCl. However, dissolution of TMR-Aβ amyloids is different from what is expected in the case of thermodynamic solubility. For example, the fraction of soluble amyloids is found to be independent of total concentration of the peptide at all concentrations of the denaturants. Additionally, soluble fraction is dependent on growth conditions such as temperature, pH, and aging of the amyloids. Furthermore, amyloids undissolved in a certain concentration of the denaturant do not show any further dissolution after dilution in the same solvent; instead, these require higher concentrations of the denaturant. Taken together, our results indicate that amyloids are a heterogeneous ensemble of metastable states. Furthermore, dissolution of each structurally homogeneous member requires a unique threshold concentration of denaturant. Fraction of soluble amyloids as a function of concentration of denaturants is found to be sigmoidal. The sigmoidal curve becomes progressively steeper with progressive seeding of the amyloids, although the midpoint remains unchanged. Therefore, heterogeneity of the amyloids is a major determinant of the steepness of the sigmoidal curve. The sigmoidal curve can be fit assuming a normal distribution for the population of the amyloids of various kinetic stabilities. We propose that the mean and the standard deviation of the normal distribution provide quantitative estimates of mean kinetic stability and heterogeneity, respectively, of the amyloids in a certain preparation.

INTRODUCTION

Alzheimer's disease (AD) is characterized by insoluble plaques of amyloid beta (Aβ) peptides in the brain (1). The primary constituents of the plaques are Aβ_{1-40} and Aβ_{1-42} with Aβ_{1-42} being the major component (2,3). In vitro, Aβ peptides have been shown to aggregate into soluble oligomers and insoluble amyloid fibrils. Although the oligomers are associated with loss of synapses (4,5), the plaques are accompanied by increased microglial activity and inflammation in the brain (6). However, there are considerable heterogeneities among both the soluble oligomers and insoluble fibrils of amyloid proteins. In vitro, amyloid fibrils are found as a highly polymorphic mixture of various forms such as single-stranded or multistranded fibrils, and sheet, rod, or twisted ribbonlike morphologies (7–10). In vivo, postmortem brain sections from AD patients show at least three distinct types of amyloid deposits such as diffuse, fibrillar, and dense core fibrillar plaques (11). Recent studies indicate that biological activities of the amyloids are related to its molecular structures (12,13). In vivo, the diffuse plaques are reported to be benign, but the fibrillar plaques are found to be associated with neurotoxicity in AD (14). In vitro, mature fibrils of Aβ peptides were found to be orders-of-magnitude more toxic than the immature types (15), but in the case of transthyretin fresh aggregates, were shown to be more toxic than the mature fibrils (16). Therefore, understanding heterogeneities of the amyloids are crucial to understand its biological activities such as toxicity. Various imaging techniques such as electron microscopy (EM), atomic force microscopy, and tip-enhanced Raman spectroscopy have been used to characterize the heterogeneous forms of the amyloids (17). However, estimation of heterogeneity of the amyloids in a certain preparation has not been possible due to lack of quantitative assays.

Here we examine whether heterogeneity of the amyloids can be characterized using its disaggregation properties. Although aggregation of amyloid proteins has been studied extensively over the past three decades, literature reports on

Submitted August 3, 2017, and accepted for publication December 11, 2017.
*Correspondence: kanchan@tifrh.res.in
Editor: James Shorter.
https://doi.org/10.1016/j.bpj.2017.12.023

disaggregation of amyloids are rare (18–20). In a few studies, disaggregation of amyloids under denaturing conditions have been used to quantify thermodynamic stability of the amyloids of several different proteins such as β2-microglobulin, SH3 domain of α-spectrin, and Aβ (18–20). The stabilities of the amyloids of several different proteins were found to be high ($\Delta G \approx -40$ kJ/mol) and quite similar to each other (20). These authors analyzed their data using a linear polymerization mechanism considering thermodynamic equilibrium between the monomers and the amyloid aggregates. Although amyloids prepared under specific conditions may exhibit thermodynamic equilibrium with the monomers, it may not be common for most of the amyloids (20). Instead, amyloid aggregates are known to exhibit properties peculiar to metastable systems (21). Hence, disaggregation of amyloids may not be governed by thermodynamic stability alone; rather, it may be influenced by the kinetic stabilities and the underlying heterogeneity.

Here we examine kinetics and thermodynamics of dissolution of amyloid aggregates of TMR-Aβ42 in chemical denaturants such as urea and guanidinium chloride (GdnCl). To monitor disaggregation, we have used recovery of TMR fluorescence based on the assay developed by Garai and Frieden (22). These authors demonstrated that quenching of TMR fluorescence can be used to monitor amyloid aggregation of TMR-Aβ. Our results suggest that dissolution properties of amyloid aggregates are different from those of small molecules; amyloids share properties of polymer glasses. TMR-Aβ amyloids consist of a heterogeneous mixture of metastable forms that differ in terms of apparent solubility or kinetic stability in denaturing solvents. Interconversion between these states is extremely slow, enabling us to determine the distribution of the aggregates in terms of kinetic stabilities to provide a quantitative description of the heterogeneity of the amyloids.

MATERIALS AND METHODS

Purification of tetramethylrhodamine-labeled $A\beta_{1-42}$

Chemically synthesized tetramethylrhodamine (TMR)-labeled $A\beta_{1-42}$ (TMR-Aβ42) was purchased from Aapptec (Louisville, KY). In this peptide, the TMR moiety is attached to the N-terminal amine of the peptide. This peptide is quite similar to the TMR-labeled Aβ used previously by Garai and Frieden (22). These authors used a TMR-K-Aβ where the TMR was attached to the side chain of an extra lysine residue at the N-terminal of the peptide (22). We have examined the kinetics of aggregation of the peptide by TMR fluorescence and structural properties of the aggregates by circular dichroism and atomic force microscopy. Fig. S1, *A–C*, shows that the aggregation behavior of our peptide is similar to those reported by Garai and Frieden (22). All other chemicals were purchased from Sigma-Aldrich (St. Louis, MO). Lyophilized peptide (~5 mg) was dissolved in 200 μL of formic acid (Merck, Kenilworth, NJ) in an ice bath. Dissolved peptide was precipitated by adding the solution to 10 mL of ice-cooled 500 mM Tris buffer (pH = 8.0). Precipitated peptide was pelleted down by centrifugation at 4500 × *g* (Eppendorf, Hamburg, Germany) for 15 min at 4°C. The pellet was dissolved in 2 mL of 6 M GdnCl. It was then purified by size exclusion chromatography using a Superdex peptide column (GE Healthcare, Little Chalfont, UK) in 4 M GdnCl containing 10 mM phosphate-buffered saline (PBS, pH 7.4), 5 mM β-mercaptoethanol (βMe), and 1 mM EDTA. Only the monomeric fractions were collected. The GdnCl was removed by buffer exchange to 5 mM NaOH containing 5 mM βMe and 1 mM EDTA using a PD10 column (GE Healthcare). The sample was distributed in 100 μL aliquots, which were then flash-frozen in liquid nitrogen and stored at −80°C.

Preparation of TMR-Aβ amyloid fibril stock

A 6 μM TMR-Aβ42 peptide solution was prepared in 20 mM phosphate buffer, pH 7.4 containing 150 mM NaCl, 5 mM βMe, and 1 mM EDTA. The peptide was incubated at 37°C in a glass tube with continuous stirring at 400 RPM using a micro stirrer bar. Kinetics of aggregation was monitored using TMR fluorescence with a fluorometer (Photon Technology International, Princeton, NJ). The kinetics were found to be similar to what were reported by Garai and Frieden (22) (see Fig. S1 *A*). Excitation and emission were set at 550 and 585 nm, respectively. Upon completion of aggregation, the aggregates were separated from the soluble part by centrifugation at 16,000 × *g*. Supernatant concentration was calculated by measuring its absorbance at 555 nm. The stock fibril solution was prepared by resuspending the pellet in 10 mM PBS, pH 7.4 containing 5 mM βMe and 1 mM EDTA. Fibril stock concentration was calculated by subtracting supernatant concentration from the initial concentration. The secondary structure of the fibril stock was verified by circular dichroism and the morphology by atomic force microscopy (see Fig. S1, *B* and *C*). For preparation of the amyloids at different temperatures and pH conditions, the TMR-Aβ42 solutions were incubated at the respective temperatures in phosphate buffers of appropriate pH values. It may be noted here that upon prolonged incubation at 37°C there is a possibility of hydrolysis of dye from the peptide. This has been taken care of by removing the supernatant after aggregation and by washing the pellet.

Disaggregation kinetics of TMR-Aβ42 amyloids using fluorescence correlation spectroscopy

A home-built fluorescence correlation spectroscopy (FCS) setup was used to perform FCS measurements. The FCS autocorrelation data were fit assuming a single diffusing species using the following equation (23):

$$G(\tau) = \frac{1}{N\left(1+\frac{\tau}{\tau_D}\right)\left(1+\frac{\tau}{\gamma^2\tau_D}\right)^{1/2}}, \quad (1)$$

where N is the average number of molecules inside the FCS observation volume, τ_D is the diffusion time of the molecule, and γ is the ratio of the axial and radial dimensions of the FCS observation volume. The observation volume of the FCS setup was calibrated using a 25 nM Rhodamine B (RB) solution. Hydrodynamic radius of TMR-Aβ42 ($R_{h,A\beta}$) was calculated from the ratio of the measured diffusion times (τ_D) of TMR-Aβ42 and RB using:

$$(R_h)_{A\beta} = (R_h)_{RB} \times \frac{\tau_{D,\,A\beta}}{\tau_{D,\,RB}}. \quad (2)$$

Hydrodynamic radius of RB ($R_{h,RB}$) is equal to 0.58 nm (24). Diffusion time of monomeric Aβ was measured using a 25 nM TMR-Aβ42 solution collected from the monomer fraction in size exclusion chromatography. The FCS measurements in 4 M GdnCl were performed by keeping the FCS observation volume within 5 μm inside the solution from the glass coverslip to avoid optical aberrations due to refractive index mismatch. Kinetic experiments on disaggregation of amyloids were performed by 200-fold dilution of a 12 μM TMR-Aβ42 fibril stock solution in PBS buffer

in the absence or in the presence of 4 M GdnCl. FCS measurements were performed continuously. Each autocorrelation was recorded for 30 s.

Disaggregation of TMR-Aβ amyloids by chemical denaturants

Kinetics of disaggregation of the amyloids of TMR-Aβ42 were monitored by using fluorescence of TMR after dilution of a 3 μM fibril stock solution to a final concentration of 30 nM in 0–7 M GdnCl or 0–9 M Urea in 10 mM PBS, pH 7.4 containing 5 mM βMe and 1 mM EDTA. These experiments were performed in a 3.5 mL quartz cuvette (Fireflysci Cuvette Shop, Staten Island, NY). TMR fluorescence was monitored continuously for ~30 min. For experiments requiring long incubation times, the samples were prepared in glass tubes (i.d. = 10 mm). Samples containing urea were discarded after 2 days of incubation to avoid artifacts arising due to slow degradation of urea.

Preparation of TMR-Aβ42 fibrils by progressive seeding

A 4.4 μM of TMR-Aβ42 peptide solution was prepared in 20 mM phosphate buffer, pH 7.4 containing 150 mM NaCl, 5 mM βMe, and 1 mM EDTA. This solution was incubated at 37°C in a glass tube for 5 days to make the first generation (unseeded) of the fibrils. Seeded fibrils were prepared by incubation of fresh 4.4 μM of TMR-Aβ42 solution in presence of 10% seeds from the previous generation.

RESULTS

Dissolution of TMR-Aβ42 amyloids using FCS

Garai and Frieden (22) and Garai et al. (25) have previously shown that fluorescence of TMR can be used to monitor aggregation of TMR-Aβ monomers into soluble oligomers and insoluble fibrils. Now we examine whether this assay can be employed to monitor disaggregation of the TMR-Aβ amyloids quantitatively. Hence, we use FCS to monitor the time course of fluorescence, concentration, and hydrodynamic radii (R_h) of the soluble forms of TMR-Aβ. The values of the concentrations and the R_h are obtained from the analysis of the FCS autocorrelation data, $G(\tau)$ using Eq. 1. First, we examine if the amyloid fibrils can be solubilized by dilution in the native buffer. A 12 μM fibrillar stock is diluted to 60 nM in PBS buffer. FCS measurements are then performed continuously on the diluted sample. Fig. 1 *A* shows that the amplitudes of autocorrelation traces at time, $t = 0$, i.e., $G(0)$ decrease with time by a small extent (from 1.0 to 0.8) indicating a small increase in the concentration of soluble TMR-Aβ. The autocorrelation curves are then analyzed using Eq. 1 to determine concentration and hydrodynamic radii (R_h) of the dissolved species. Fig. 1 *B* shows that the fluorescence count rate (*squares*) increases from 20 to 28 kHz and the concentration (*circles*) of soluble TMR-Aβ increases from 1.0 to 1.4 nM. The increase of both fluorescence and the concentration are small, but these are in good agreement with each other. Fig. 1 *C* shows that values of the R_h remain constant at 1.63 nm ($\pm$0.03 nm), which corresponds to the size of the monomeric TMR-Aβ in PBS (see Fig. S2 *A*). Therefore, Fig. 1, *A–C*, indicate a very small amount of dissolution of the amyloid fibrils to monomeric peptide in the native

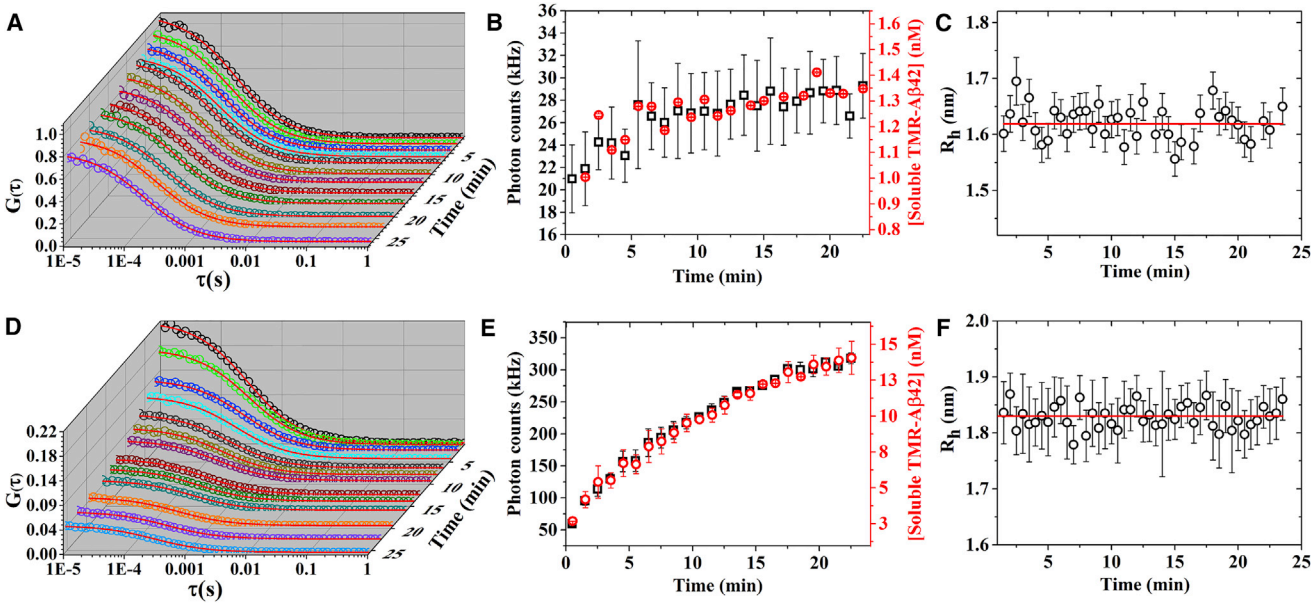

FIGURE 1 Disaggregation of TMR-Aβ42 amyloids monitored by FCS in PBS (*A–C*) and in 4 M GdnCl (*D–F*). (*A* and *D*) FCS autocorrelation data, $G(\tau)$ (*open circles*) and the fits using Eq. 1 assuming single diffusing species (*solid lines*). Autocorrelation data were recorded every 30 s. However, traces recorded every 2 min are shown here for clarity of presentation. (*B* and *E*) Photon count rates (*squares*) and concentrations (*circles*) obtained from analysis of the autocorrelation data. (*C* and *F*) Circles represent hydrodynamic radii (R_h) obtained from analysis of the autocorrelation data, and the solid lines represent the mean of all the measured values of R_h. Total concentration of amyloids used here is 60 nM (monomer equivalent). Clearly, R_h of solubilized TMR-Aβ corresponds to the size of the monomeric peptide (see Fig. S2). To see this figure in color, go online.

buffer. We then examine the dissolution of the TMR-Aβ fibrils in 4 M GdnCl. Fig. 1 *D* shows that amplitudes of the FCS autocorrelation trace, i.e., G (0) decrease from 0.2 to 0.04 in 25 min. Fig. 1 *E* shows that fluorescence count rate increases from 60 to 300 kHz and the concentration of the soluble TMR-Aβ increases from 3 to 15 nM. It may be noted here that at time, $t \approx 0$, $G(0)$ is less and the count rate is higher in 4 M GdnCl compared to the respective values obtained in native buffer. Therefore, disaggregation of the amyloids in GdnCl occurs in at least two phases. First, there is a fast dissolution that occurs within the mixing time (<3 s) of the solution and then there is a slow dissolution. Once again, good agreement can be observed between the time courses of the count rate and the soluble concentration of TMR-Aβ. Fig. 1 *F* shows that the values of R_h remain constant at 1.83 nm ($\pm$0.02 nm), which corresponds to the value of R_h obtained for monomeric TMR-Aβ in 4 M GdnCl (see Fig. S2 *B*). We note here that there is ~10% increase of the R_h of TMR-Aβ in 4 M GdnCl compared to that of in the native buffer, indicating a small amount swelling of the peptide in GdnCl. Overall, the data presented in Fig. 1 indicate that TMR-Aβ fibrils dissolve significantly in 4 M GdnCl, but minimally in the native buffer. The increase of TMR fluorescence is proportional to the increase of the concentration of TMR-Aβ monomers. Therefore, fibrils or the oligomers do not contribute to the TMR fluorescence significantly. In the subsequent experiments, TMR fluorescence has been used as a measure of the concentration of monomeric TMR-Aβ in solution.

Kinetics of dissolution of TMR-Aβ42 amyloids as a function of denaturant concentrations

We then investigate the kinetics of dissolution of the TMR-Aβ amyloids as a function of the concentrations of the chemical denaturants such as urea and GdnCl. A 3 μM stock solution of TMR-Aβ fibrils is diluted 100-fold in PBS buffer containing different concentrations of urea or GdnCl. Kinetics of dissolution are monitored continuously using TMR fluorescence. Fig. 2, *A* and *D*, shows that kinetics of dissolution of TMR-Aβ amyloids are faster in higher concentrations of both urea and GdnCl. There is significant dissolution of the amyloids within the mixing time of the solutions at higher concentrations of GdnCl, indicating faster dissolution in GdnCl than in urea. The increase of fluorescence is minimal below 2 M urea or 1 M GdnCl, indicating extremely slow disaggregation of the amyloids at low denaturant concentrations.

We then calculate the apparent rate constants of disaggregation (k_-) at the initial time from kinetic data presented in Fig. 2, *A* and *D*. The k_- is calculated using the following expression:

$$k_- = \frac{1}{C_{\text{total}}}\frac{dC}{dt} = \frac{1}{C_{\text{total}}}\frac{C(t) - C(0)}{t}. \qquad (3)$$

Here $C(t)$, $C(0)$ indicate concentrations of dissolved monomers at time $= t$ and 0, respectively. C_{total} is the total concentration of the amyloids (monomer equivalent). Fig. 2, *B* and *E*, shows that ln(k_-) varies linearly with

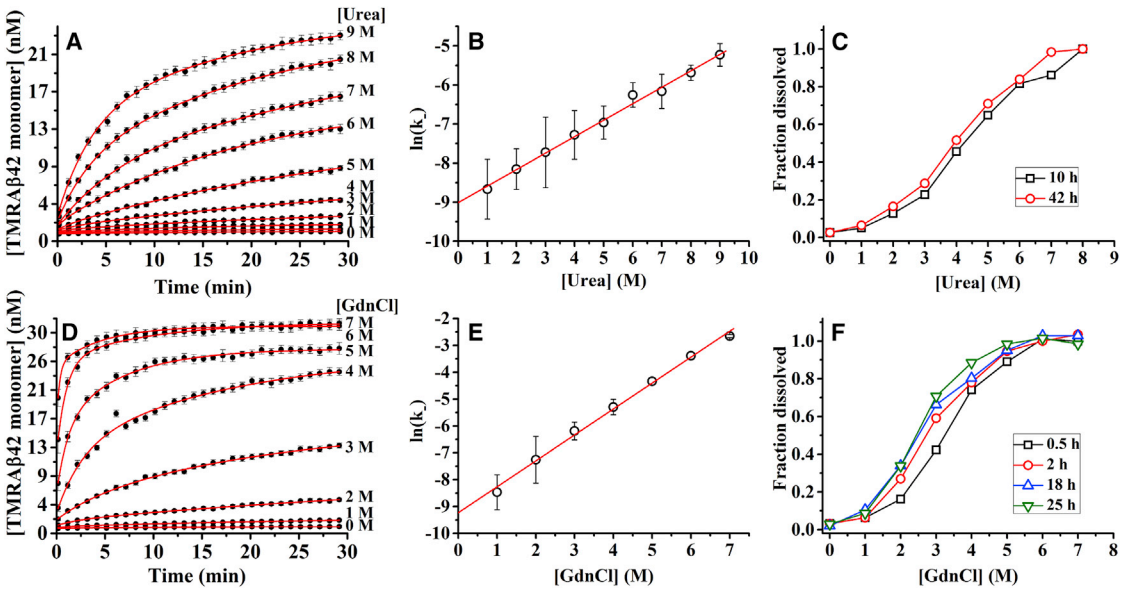

FIGURE 2 Time course of disaggregation of TMR-Aβ42 amyloids in urea (*A–C*) and in GdnCl (*D–F*) monitored by TMR fluorescence. (*A* and *D*) Kinetics of disaggregation in 0–9 M urea (and in 0–7 M GdnCl). Solid lines are fits using double exponentials. (*B* and *E*) Natural logarithm of apparent initial rate constants of disaggregation ($ln(k_-)$) calculated using Eq. 3 from the kinetic data. Solid lines are linear fits. (*C* and *F*) Fraction of dissolved peptide measured at different time points between 10 and 42 h for urea (and between 0.5 and 25 h for GdnCl). Disaggregation reaches near completion within 42 h in urea and 18 h in GdnCl. The concentration of amyloids used here is 30 nM (monomer equivalent). To see this figure in color, go online.

concentrations of both urea and GdnCl. Here k_{-} has been calculated using $t = 10$ s. Hence, disaggregation of the amyloids increases exponentially with concentration of denaturants. Using linear extrapolation, the calculated disaggregation rate constants in PBS ($k_{-,PBS}$) are equal to $(1.23 \pm 0.01) \times 10^{-4}$ and $(1.01 \pm 0.01) \times 10^{-4}$ s^{-1} from Fig. 2, *B* and *E*, respectively.

Fig. 2, *C* and *F*, show the fraction of TMR-Aβ amyloids dissolved as a function of concentration of urea (and GdnCl) measured at different time points. The soluble fraction shows sigmoidal dependence with the concentrations of denaturants. The sigmoidal dependence generally indicates cooperativity of the process. Furthermore, soluble fractions of TMR-Aβ in intermediate concentrations of the denaturants increase with time over several hours. However, the disaggregation seems to reach near completion within 42 and 18 h of incubation in urea and GdnCl, respectively. Therefore, disaggregation of amyloids is an extremely slow process, particularly at lower concentrations of the denaturants.

Soluble concentration as a function of total concentration of the amyloids, $C_{soluble}$ versus C_{total}

We then examine if the dissolution of the TMR-Aβ amyloids reaches thermodynamic equilibrium so that the dissolved concentrations may be considered as the thermodynamic solubility of the amyloid peptides under the particular solvent conditions. To test thermodynamic solubility, we examine the relationship between total concentration (C_{total}) and the soluble concentration ($C_{soluble}$) of the amyloids. Concentrations (monomer equivalent) of the amyloids used in these solutions are 25, 50, 99, 197, and 389 nM. Fig. 3 *A* shows that the dissolved TMR-Aβ concentration increases proportionally to the amounts of amyloids added ($C_{soluble} \propto C_{total}$) at all the concentrations of GdnCl. The constant of proportionality is ≈ 0 at 0 M and is ≈ 1 at 6 M GdnCl. This is contrary to what is expected in the case of dissolution governed by thermodynamic solubility. Fig. S3 presents an example of the expected behavior when a small molecule such as tyrosine is dissolved in GdnCl. As expected in the case of thermodynamic solubility, these plots have two distinct regimes: 1) for $C_{total} < C_{sat}$, $C_{soluble} = C_{total}$ and 2) for $C_{total} > C_{sat}$, $C_{soluble} = C_{sat}$. Here, C_{sat} refers to saturation concentration. Therefore, dissolution of the amyloids does not reach thermodynamic solubility. We then replot the data presented in Fig. 3 *A* in terms of fraction of fibrils dissolved, $C_{soluble}/C_{total}$ as a function of the GdnCl concentration. Fig. 3 *B* shows that these plots are sigmoidal in nature, similar to the observations presented in Fig. 2, *C* and *F*. Furthermore, fraction of the fibrils dissolved for all of the different total concentrations of the TMR-Aβ fibrils overlap with each other. Hence, fraction of the fibrils dissolved at any particular concentration of GdnCl is independent of total concentration of the amyloids indicating metastability and heterogeneity of the amyloids (26).

Dissolution of aggregates prepared in different temperature, pH, and incubation time

To verify metastability of the amyloids further, we compare dissolution properties of the amyloid aggregates prepared under different solution and incubation conditions. Hence, we prepare the amyloid aggregates under different solution and incubation conditions, but the dissolution experiments have been performed under the same solvent conditions, i.e., in PBS buffer containing GdnCl at room temperature. Fig. 4 *A* shows the fraction of dissolved fibrils that have been prepared at different temperatures, i.e., at 25 and 37°C as a function of GdnCl concentration. These plots show that the fibrils prepared at higher temperatures are more stable than those that are prepared at lower temperatures, although the differences are small. Fig. 4 *B* compares the stabilities of the fibrils prepared in phosphate buffers at pH 5.7 and 7.4. Clearly, fibrils prepared at lower pH are less stable. Fig. 4 *C* shows that the denaturation of the amyloids,

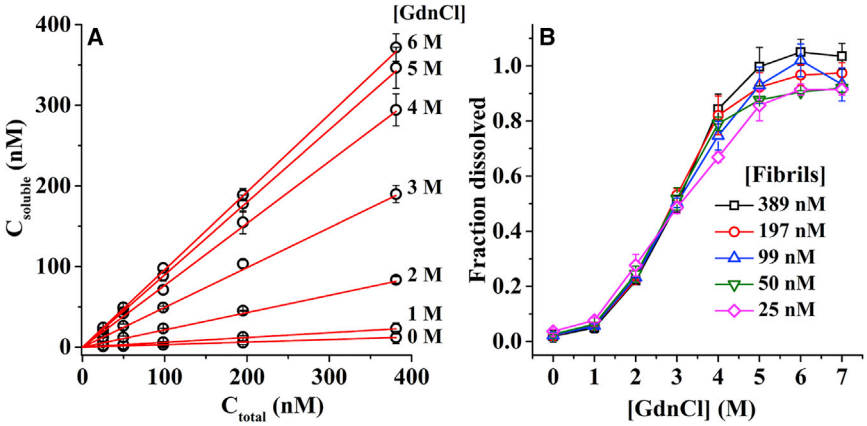

FIGURE 3 Relationship between soluble ($C_{soluble}$) and total concentrations (C_{total}). (*A*) $C_{soluble}$ versus C_{total} of TMR-Aβ fibrils in 0–6 M GdnCl; open circles represent the data and solid lines are linear fits. Soluble peptide concentrations were calculated from TMR fluorescence. (*B*) Soluble fraction ($C_{soluble}/C_{total}$) as a function of GdnCl concentration. Clearly, fraction dissolved (i.e., $C_{soluble}/C_{total}$) is independent of the total concentration of the amyloids. Total concentrations of amyloids used here are 25, 50, 99, 197, and 389 nM. To see this figure in color, go online.

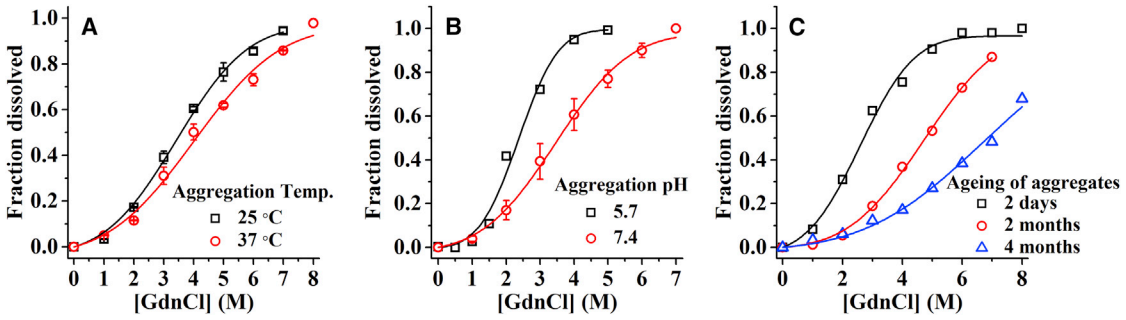

FIGURE 4 Effects of temperature, pH, and aging on stability of the TMR-Aβ amyloids. (*A*) Soluble fraction as a function of [GdnCl] for amyloids prepared at 25°C (*square*) and 37°C (*circle*). (*B*) Amyloids prepared at pH 5.7 (*square*) and pH 7.4 (*circle*). (*C*) Amyloids aged for 2 days (*square*), 2 months (*circle*), and 4 months (*triangle*). Solid lines are fits using Eq. 5. Clearly, soluble fractions depend strongly on preparation conditions. Concentration of amyloids used here is 50 nM (monomer equivalent). To see this figure in color, go online.

which have been incubated in PBS at 37°C for 2 days, and 2 and 4 months. It is clear that stability of the amyloids increases with aging of the fibrils, indicating slow evolution of the fibrils into more stable structures (27,28). Most strikingly, aggregates that are aged for 4 months could not be dissolved well even in 8 M GdnCl. Taken together, apparent solubility of TMR-Aβ amyloids depend strongly on the preparation conditions. Therefore, amyloids may reach different metastable state(s) depending on the growth conditions.

Kinetics of dissolution of the fibrils preincubated in GdnCl

We then examine heterogeneity of the amyloids further by comparing the kinetics of disaggregation of TMR-Aβ amyloids that have been preincubated in different concentrations of GdnCl. Fig. 5 *A* shows the time course of TMR fluorescence when TMR-Aβ amyloids that have been preincubated in 3 M GdnCl are diluted 50-fold in 3–6 M GdnCl. It may be seen that the TMR fluorescence does not increase at all in 3 M GdnCl, indicating no further dissolution within the experimental time. However, these fibrils can be dissolved further at higher concentrations of GdnCl. Similarly, Fig. 5 *B* shows that fibrils preincubated in 4 M GdnCl do not dissolve noticeably in 4 M GdnCl; rather, these require higher concentrations of GdnCl for dissolution. Furthermore, Fig. 5, *A* and *B*, shows that kinetics of disaggregation of the preincubated fibrils at any concentration of GdnCl are much slower compared to kinetics observed in the case of fibrils incubated in native buffer (see Fig. 2 *D*). Hence, dissolution behaviors of the fibrils incubated in 0, 3, and 4 M GdnCl are different from each other, indicating heterogeneity and metastability of the fibrils. Furthermore, amyloids preincubated in a certain concentration of GdnCl exhibit no further dissolution after dilution in the same concentration of GdnCl. Hence, each structurally homogeneous state of the amyloids requires a specific threshold concentration of GdnCl for dissolution. Dissolution of the fibrils is extremely slow below the required threshold concentration of the denaturant. Therefore, disaggregation of each homogeneous state is a highly cooperative process.

Effects of progressive seeding on denaturant-dependent apparent solubility of the amyloids

Progressive seeding of amyloid fibrils is known to reduce the heterogeneity of fibril preparations (8,29). We now examine how progressive seeding of the amyloids affects its apparent solubility. Fig. 6 shows the effects of progressive seeding on the GdnCl-dependent soluble fraction of the TMR-Aβ amyloids. The amyloids used in these

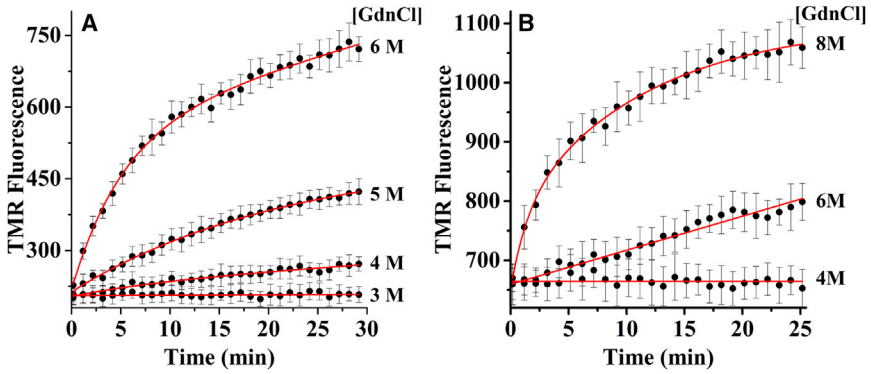

FIGURE 5 Time course of disaggregation of TMR-Aβ42 amyloids preincubated in 3 M (*A*) and 4 M GdnCl (*B*). Aliquots of 5 μM amyloid fibril stock were preincubated in 3 and 4 M GdnCl for 24 h at RT. Kinetics of TMR fluorescence were recorded after 50-fold dilution of the GdnCl-incubated amyloids in different concentrations of GdnCl. The symbols represent data and the solid lines are guide for the eye. Clearly, the amyloids preincubated in 3 M (or 4 M) GdnCl do not dissolve any further in 3 M (or 4 M) GdnCl. Kinetics observed here is much slower than those observed in Fig 2, *A* and *D*. To see this figure in color, go online.

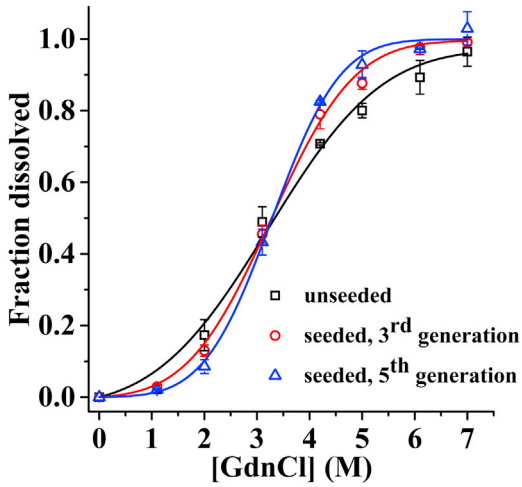

FIGURE 6 Effects of progressive seeding on denaturant-dependent disaggregation of amyloids. Soluble fraction ($C_{soluble}/C_{total}$) as a function of [GdnCl] using TMR-Aβ42 amyloids prepared without seeding (*squares*) and with third generation (*circles*) and fifth generation (*triangles*) of progressive seeding. Solid lines are fits using Eq. 5. Clearly, steepness of the sigmoid curves increases with progressive seeding whereas the midpoints remain unchanged. To see this figure in color, go online.

experiments have been prepared with no seeding, and with a third and fifth generation of seeding. Clearly, the sigmoidal curves become progressively steeper with successive seeding, whereas the midpoints of the curves remain the same. Therefore, the data presented above are consistent with the midpoint and the steepness of the sigmoidal being a measure, respectively, of mean stability and heterogeneity of the amyloids.

Denaturant-mediated dissolution as a measure of stability and heterogeneity of the aggregates

The data presented above indicate that amyloids consist of a heterogeneous assembly of metastable states. Each member of the heterogeneous ensemble, i.e., each structurally homogeneous state, has a unique kinetic stability. Therefore, we propose that each member of the ensemble of the heterogeneous amyloids may be characterized on the basis of its kinetic stability measured by the threshold concentration of denaturant (ρ^*) required for its dissolution. For quantitative evaluation of the heterogeneity, we assume that the distribution of the population in a certain preparation of the amyloids is Gaussian. Hence the normalized population distribution $P(\rho^*)$ can be expressed as

$$P(\rho^*) = \frac{1}{\sigma\sqrt{2\pi}} e^{-\frac{1}{2}\left(\frac{\rho^* - \langle\rho\rangle}{\sigma}\right)^2}, \quad (4)$$

where $\langle\rho\rangle$ is the mean and σ is the standard deviation (SD) of the distribution. In the context of amyloids, $\langle\rho\rangle$ and σ signify mean stability and heterogeneity, respectively. The fraction of peptide dissolved at any particular concentration, ρ, of GdnCl can be expressed as follows:

$$C_{soluble}(\rho) = \frac{1}{\sigma\sqrt{2\pi}} \int_0^{\rho} e^{-\frac{1}{2}\left(\frac{x - \langle\rho\rangle}{\sigma}\right)^2} dx$$
$$= \frac{1}{2}\left[\mathrm{erf}\left(\frac{\rho - \langle\rho\rangle}{\sqrt{2}\sigma}\right) + \mathrm{erf}\left(\frac{\langle\rho\rangle}{\sqrt{2}\sigma}\right)\right], \quad (5)$$

where the error function is defined as $\mathrm{erf}(z) = 2/\sqrt{\pi}\int_0^z e^{-u^2}\mathrm{d}u$.

We then examine if the data presented in Figs. 4 and 6 can be fit using Eq. 5. Solid lines in Figs. 4, *A–C* and 6 are fits of the denaturant-dependent apparent solubility data using Eq. 5. Clearly, the disaggregation data fit well, indicating agreement with the Gaussian distribution for ρ^*. The values of $\langle\rho\rangle$ and σ obtained from the analysis are summarized in Tables S1 and S2. The normal distributions as described in Eq. 4 using the determined values of $\langle\rho\rangle$ and σ are plotted in Fig. 7, *A–D*. Fig. 7, *A–C*, shows that both the mean and the SD of the distributions increases with an increase in temperature, pH, and aging—indicating an increase in both stability and heterogeneity. Fig. 7 *D* shows that the distributions of the amyloids become narrower with progressive seeding, although the mean remains the same.

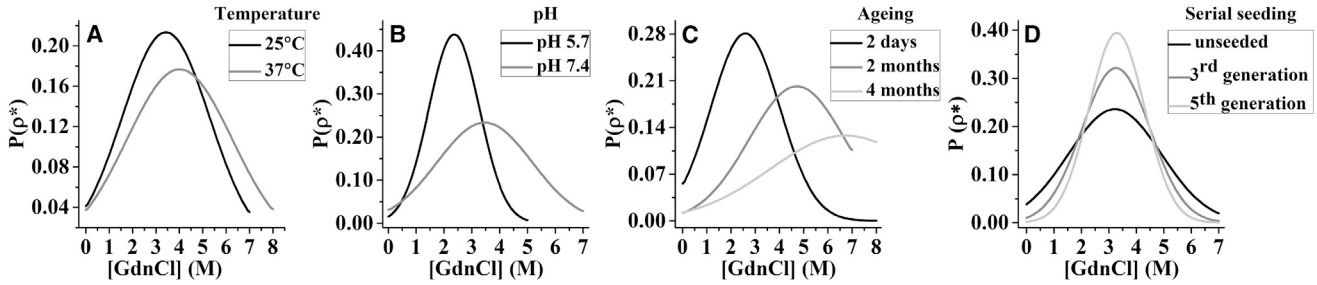

FIGURE 7 Distribution of the amyloids classified based on the threshold concentration of GdnCl (ρ^*_{GdnCl}) required to dissolve a particular homogeneous population of the amyloids. Gaussian distributions (Eq. 4) are calculated using the values of $\langle\rho\rangle$ and σ obtained from fitting of the data presented in Figs. 4, *A–C*, and 6 using Eq. 5 (see Tables S1 and S2). Clearly, the distributions shift to higher stabilities from 25°C to 37°C (*A*), from pH 5.7 to pH 7.4 (*B*) and with aging from 2 days to 4 months (*C*). The distribution becomes narrower with progressive seeding whereas the mid points remain the same (*D*).

DISCUSSION

There is much debate in the literature about whether amyloid fibrils are cytotoxic or harmless byproducts in protein aggregation diseases (30). This debate is fueled by observations that severity of the disease in AD does not correlate well with the load of the amyloid plaques in the brain (31,32). However, numerous evidences indicate that amyloid fibrils could exert their cytotoxic properties via diverse pathways. For example, the amyloid fibrils can cause disruption of cellular membranes (33) or act as reservoirs for toxic soluble oligomers as the oligomers may form by secondary nucleation and fragmentation (32,34,35). Amyloid fibrils can also be the primary agent responsible for transmission of amyloids from cell-to-cell or individual-to-individual due to its high stability and strong resistance to proteolytic degradation (36,37). However, mechanisms of toxicity of the fibrils are still unclear. A major reason behind this is the highly polymorphic nature of the fibrils (30). Polymorphic forms of the fibrils are known to differ in terms of length distribution, mechanical stability, and biological activities (8,38,39). Therefore, although some forms of the amyloids may be cytotoxic, some other forms of the amyloids of the same peptide may be benign—leading to conflicting observations regarding the toxicity of the amyloids (15,16). Hence, characterization of the heterogeneity of the amyloid aggregates is important to unravel the mechanisms of its diverse biological activities.

Disaggregation and clearance of amyloid deposits of Aβ have been the major targets of the clinical trials in AD (40,41). However, kinetics or thermodynamics of disaggregation of amyloids are poorly understood. Although aggregation of amyloid proteins has been studied extensively, there are only a few studies on disaggregation of the amyloids (18–20). For example, a large number of small molecules are known to inhibit amyloid aggregation (42–44), but very few molecules have been found to cause disaggregation of amyloids (45,46). A major difficulty in studying disaggregation is that amyloids are known to be extremely stable, sometimes practically insoluble even under strongly denaturing conditions. The origin of high stability of the amyloids is not well understood, but it is generally believed to arise from the extensive intra- and intermolecular H-bonding and hydrophobic interactions (19,47). Studies on disaggregation of the amyloids can shed light on the stability of the amyloids. This can potentially help to design small molecules to disrupt the amyloids. Furthermore, it can help to design highly stable amyloid fibrils for applications in nanobiotechnology (48). In this article, we have studied the kinetics of disaggregation of the TMR-Aβ amyloids to examine whether disaggregation properties can be used to characterize heterogeneity and thermodynamic or kinetic stability of the amyloids.

TMR fluorescence is a sensitive assay to monitor disaggregation of amyloids

Garai and Frieden (22) have previously shown that fluorescence of TMR-Aβ can be used to monitor aggregation of this peptide or disaggregation of these amyloids (25). TMR fluorescence has also been used to monitor aggregation of TMR-labeled polyglutamine (49). Here we have performed FCS measurements to check how quantitative this assay is. Our FCS data presented in Fig. 1 show that the hydrodynamic radius of the dissolved species is identical to the monomeric peptide (see Fig. S2). Furthermore, the fluorescence is proportional to the number of molecules in the FCS observation volume (Fig. 1, *B* and *E*). Hence, TMR fluorescence is proportional to the concentration of monomeric TMR-Aβ in the solution. In other words, contributions of oligomeric or fibrillar aggregates to the total TMR fluorescence are negligible. We note here that this approach does not require any physical separation of the monomer population from the self-assembled forms. Previous studies have used Thioflavin T fluorescence to measure the content of the fibrils (28,50). However, ThT assay is not quantitative. Hence, these observations are generally supplemented with EM or AFM imaging. TMR fluorescence assay, on the other hand, is quantitative and highly sensitive to even subnanomolar concentrations.

Dissolution of TMR-Aβ amyloids versus thermodynamic solubility

Fig. S3 shows the relationship between soluble versus total concentration, as expected in the case of thermodynamic solubility using a small molecule tyrosine. It can be seen that $C_{\text{soluble}} = C_{\text{total}}$ for $C_{\text{total}} < C_{\text{sat}}$ and $C_{\text{soluble}} = C_{\text{sat}}$ for $C_{\text{total}} > C_{\text{sat}}$. Here C_{soluble}, C_{sat}, and C_{total} indicate soluble, saturation, and total concentrations, respectively. However, Fig. 3 shows that this is not the case for TMR-Aβ amyloids. Here we find that $C_{\text{soluble}} \propto C_{\text{total}}$, i.e., $C_{\text{soluble}}/C_{\text{total}} =$ constant over a range of concentrations of TMR-Aβ amyloids. Therefore, dissolution of the amyloids does not reach thermodynamic solubility within the time of the experiments, i.e., in several days.

Metastability and heterogeneity of the amyloids

The data presented in Fig. 3 show that $C_{\text{soluble}}/C_{\text{total}}$ is independent of C_{total}, indicating that the amyloids are metastable and heterogeneous (26). Metastability of the amyloids is further evident from the data presented in Fig. 4, which suggest that the soluble fraction depends also on aggregation conditions such as temperature, pH, and aging. Aβ aggregates prepared at pH close to 5.5 are known to be more amorphous or disordered than fibrillar (51). Therefore, pH-dependent apparent solubility data indicate that amorphous aggregates may be less stable compared to the

fibrillar forms (52). The effect of aging is particularly striking. Whereas nascent amyloids are dissolved completely in 6 M GdnCl, the 4-month-old samples could not be dissolved well even in 8 M GdnCl. Therefore, amyloid aggregates mature slowly to more stable forms. For example, using multidimensional infrared spectroscopy, Ma et al. (27) have shown that structures of the amyloids evolve over several years. Furthermore, higher stability of the amyloids prepared at 37°C than those prepared at RT (see Fig. 7 *A*) occur probably due to faster maturation of the amyloids at higher temperature. Therefore, our results indicate that amyloids grown under different conditions may give rise to different metastable state(s).

Heterogeneity of the amyloids is further supported by the data presented in Fig. 5 that indicate that amyloids preincubated in 3 or 4 M GdnCl do not dissolve noticeably within the time of the experiments in the same concentration of GdnCl even after 50-fold dilution. Preincubated amyloids can be dissolved further only in higher concentrations of GdnCl, but the kinetics of dissolution are much slower than those observed in the case of aggregates not incubated in GdnCl (see Fig. 2 *D*). These observations are consistent with the explanation that the amyloids undissolved during the preincubation period are kinetically insoluble in that concentration of GdnCl. Therefore, amyloids are a heterogeneous mixture of metastable states. Dissolution of each member, i.e., each structurally homogeneous state, requires a unique threshold concentration (ρ^*) of the denaturant. Dissolution is extremely slow below the threshold concentration. Requirement of a threshold concentration of the denaturant indicates high cooperativity of the disaggregation process. Therefore, we propose that the various structural states of the amyloids may be characterized in terms of kinetic stabilities that can be measured in terms of ρ^* of a denaturant such as GdnCl.

A schematic model of dissolution of the amyloids in chemical denaturants

Fig. 8 presents a simplified scheme to explain the observations reported in this article. In this scheme, dissolution behavior of the TMR-Aβ amyloids is explained by considering three peculiar features of the amyloids. First, amyloids are a mixture of heterogeneous and metastable states. Second, a unique threshold concentration of GdnCl is required for dissolution of each homogeneous state within the experimental time; therefore, aggregates and the monomeric peptides are separated by large kinetic barriers. Third, interconversion between the different forms of the aggregates is extremely slow. Hence, various states of the amyloids are separated by large kinetic barriers between them. Thermodynamic free energies (ΔG) also must be different for the various different states. However, dissolution of the amyloids reported here is primarily limited by the kinetic barriers. In Fig. 8, we have presented a simple picture of the amyloids

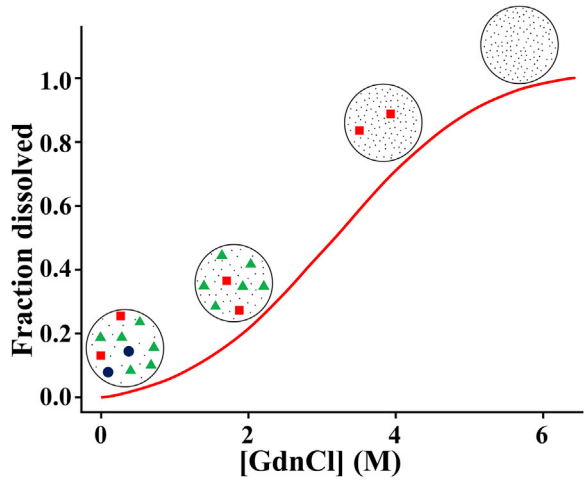

FIGURE 8 A simplified scheme for denaturant-dependent disaggregation of amyloids. Circles, triangles, and squares represent three structurally distinct metastable states of the amyloids. Dots represent monomeric peptides. Here threshold concentrations (ρ^*) of GdnCl required for disaggregation of circles, triangles, and squares are 2, 4, and 6 M respectively. Shape of the sigmoidal curve depends on the stabilities and the population distribution of the structurally distinct forms of the amyloids. To see this figure in color, go online.

consisting of three structurally distinct states represented as circles, triangles, and squares. We have assumed here that the threshold concentrations (ρ^*) of GdnCl required to dissolve the circles, triangles, and the squares are 2, 4, and 6 M of GdnCl, respectively. Therefore, at any particular concentration of GdnCl, say at 4 M GdnCl, only the circles and triangles dissolve, whereas the more stable states, such as the squares, remain undissolved. Hence, the fraction of amyloids dissolved at any particular concentration of GdnCl is constant and is determined by the relative population of the various structurally distinct states of the amyloids.

Quantitative analysis of the denaturant dependent apparent solubility of the amyloids

The schematic in Fig. 8 suggests that denaturation-dependent solubility of the amyloids contains information about the heterogeneity of the amyloids in a particular sample. The data presented in Figs. 2, 3, and 4 suggest that soluble fraction of the amyloids as a function of the concentration of GdnCl is sigmoidal. For a homogeneous system, the sigmoid curve is an indicator of cooperativity in the disaggregation process. The steepness, i.e., the slope around the midpoint of the sigmoidal curve, commonly known as the *m* value, is a measure of the cooperativity for a homogeneous system. Overall shape of the sigmoidal curve is determined by the dissociation constant (K_d) and the *m* value (19,20). However, in the presence of heterogeneity, the shape of the sigmoidal curve is the resultant of the sigmoid curves corresponding to all of the structurally homogeneous states and the underlying population distribution of those states. Therefore, a rigorous analysis of the sigmoidal curve is quite complex. Hence, we

attempt to analyze the sigmoidal curve by making a few simplified assumptions. We assume that cooperativity of the disaggregation of each homogeneous state is high. This is motivated by the observations that a threshold concentration (ρ^*) of denaturant is required for dissolution of each homogeneous state of the amyloids. Therefore, the shape of the sigmoidal curve is predominantly governed by the population distribution of the amyloids of various kinetic stabilities. This is consistent with the observations that with progressive seeding of the amyloids, there is considerable increase of the steepness of the sigmoidal curve, whereas the midpoint remains the same (see Fig. 6). Furthermore, we assume that the distribution of the amyloids of different stabilities, measured by ρ^*, is Gaussian where the mean ($\langle\rho\rangle$) and the SD (σ) correspond to mean kinetic stability and heterogeneity, respectively (see Eq. 4). Hence, the fraction of dissolved amyloids at any particular concentration of the denaturant is given by Eq. 5. Expectedly, distributions of amyloids presented in Fig. 7 show that both $\langle\rho\rangle$ and σ are dependent on the growth conditions, such as temperature, pH, aging, and seeding of the amyloids.

Our results are consistent with observations by Shih et al. (53), who found that apparent solubilities of α-chymotrypsin and BSA in sodium phosphate buffer were proportional to the total concentrations, i.e., $C_{\text{soluble}} \propto C_{\text{total}}$. Furthermore, similar observations have been reported even in the case of dissociation of oligomers of several proteins. For example, pressure-induced dissociation of the tetramers of glyceraldehydephosphate dehydrogenase and lactate dehydrogenase, and the multimers of erythrocruorin and the capsid of Brome mosaic virus, were found to be completely concentration-independent (26,54,55). In fact, pressure-induced dissociation of even the dimers of triosephosphate isomerase were found to be concentration-independent (56). The authors concluded that the oligomers constitute a "long-lived conformationally heterogeneous" population with each member having its own characteristic dissociation pressure (26). Hence, heterogeneity and high kinetic stability are probably generic properties of large assemblies of proteins.

Role of progressive seeding on the heterogeneity of the amyloids

Progressive seeding is used extensively to improve homogeneity of the fibrils for structural characterizations by ssNMR and electron microscopy (8,29). Our data in Fig. 6 and the analysis presented in Fig. 7 *D* and Table S2 suggest that progressive seeding reduces heterogeneity of the amyloids. Importantly, the midpoint of the distribution remains the same. This is consistent with the explanation that population distribution of the amyloids is a peak function and that the amyloid states corresponding to the peak grow more rapidly than the other states, thereby giving rise to sharpening of the distribution around the peak although keeping the position of the peak same. We then examined if a pure homogeneous state could be obtained in this process. Fig. S4 shows that apparent solubility of these fibrils obtained from the sixth generation of seeding in 3 M GdnCl still follows $C_{\text{soluble}} \propto C_{\text{total}}$. Therefore, several generations of progressive seeding reduce heterogeneity of the amyloids considerably, but it may not generate a pure state. Fig. 7 *C* shows that with aging, although the distribution moves toward higher stability, it also broadens. This happens most likely because, with aging, amyloids mature to new structural forms with higher stabilities, although many of the older forms may still persist, giving rise to broadening of the distribution. In fact, concomitant increase of stability and heterogeneity is observed in the case of amyloids prepared at 37°C compared to those prepared at 25°C. Because amyloids are known to grow faster at higher temperatures (22), higher stability and heterogeneity of amyloids at 37°C may arise due to faster maturation of the amyloids. Based on these observations, we speculate that heterogeneity of the amyloids originates in at least two ways. First, heterogeneities may arise due to multiple quasi-independent intermediates that form in parallel pathways. Second, heterogeneities may arise due to slow evolution or maturation of the aggregates (27). Progressive seeding may reduce the heterogeneity of the first kind, but not the second kind. Therefore, progressive seeding may never eliminate heterogeneity completely.

Nature of heterogeneity

The nature of heterogeneity of the amyloids is not fully understood but the morphologies of amyloid aggregates are known to differ significantly, depending upon preparation conditions. EM and AFM imaging have shown amyloids of diverse morphologies including globular spheroids, protofilaments, ribbonlike fibrils, and single or multistranded fibrils (10,57). Additionally, morphologically similar amyloids may also exhibit heterogeneity due to differences in the molecular conformations and the water molecules trapped inside the fibril core (27).

Similarities between dissolution of polymer glasses and amyloids

The peculiar characteristics of dissolution of the amyloid aggregates can be compared with the dissolution of polymer glasses. Physical properties of polymer glasses are determined by crystallinity, density of chain entanglements, cross linking, and the void volume (58). Generally, "cross linking" refers to covalent bonds, but in the case of amyloids, cross linking may be considered as any kind of interactions including noncovalent interactions such as hydrogen bonds and hydrophobic interactions between the amino acids. These parameters depend on the conditions of preparation of the glass (59,60). Kinetics of dissolution of a polymer glass strongly depend on the physical properties of the glass (59,61). If the kinetics is very slow compared to the

timescale of the experiments (approximately several days), it is considered effectively insoluble. Peppas et al. (62) have shown that dissolution of a polymer glass in a thermodynamically favorable solvent requires a threshold concentration (ρ^*) of the solvent. In a thermodynamically favorable solvent, the solvent molecules penetrate into the glass to form a gel. If the solvent concentration is $<\rho^*$, then the polymer chains show only segmental motions. But long-range motions, that are required for disentanglement of the polymer chains from the gel, occur at solvent concentrations $>\rho^*$. The ρ^* depends on the physical parameters of the gel (62). Therefore, dissolution of polymer glasses may strongly depend on incubation temperature, pH, and aging. This is consistent with our data, which show that dissolution of amyloids prepared under different conditions is different (see Fig. 4). Hence, an important similarity between polymer glasses and amyloids is metastability. Therefore, amyloid disaggregation characteristics are different from those of small molecule disaggregation; they actually bear similarity to those of polymer glasses.

CONCLUSION

We have characterized the disaggregation of TMR-labeled Aβ in native and denaturing aqueous buffers. We provide an experimental and phenomenological framework to estimate the kinetic stability and heterogeneities of the amyloid aggregates. In future, it would be interesting to investigate the relationship between stability and morphology of the amyloids to elucidate the molecular origin of its high stability. In this article, we have described the stability of amyloids using ρ^* of GdnCl. However, a more general approach could potentially be established by using any thermodynamically favorable solvent. In that case, the property of solvent may be expressed by using solvent quality, which is measured by the net interaction energy between the solvent and the peptide or by using solubility parameters of the solvent (63,64).

SUPPORTING MATERIAL

Supporting Materials and Methods, four figures, and two tables are available at http://www.biophysj.org/biophysj/supplemental/S0006-3495(17)35103-2.

AUTHOR CONTRIBUTIONS

T.B.S. and K.G. designed research, analyzed data, and wrote the paper. T.B.S., B.S., and S.C.B. performed research.

ACKNOWLEDGMENTS

The authors thank Prof. Rohit Pappu, Prof. Sudipta Maiti, and Dr. Pramodh Vallurupalli for insightful discussions, and Dr. Aprotim Mazumder for critical reading of the manuscript.

We acknowledge the Tata Institute of Fundamental Research and Department of Science and Technology (ECR/2015/000064) for the funding.

REFERENCES

1. Masters, C. L., G. Simms, …, K. Beyreuther. 1985. Amyloid plaque core protein in Alzheimer disease and Down syndrome. *Proc. Natl. Acad. Sci. USA.* 82:4245–4249.
2. Miller, D. L., I. A. Papayannopoulos, …, K. Iqbal. 1993. Peptide compositions of the cerebrovascular and senile plaque core amyloid deposits of Alzheimer's disease. *Arch. Biochem. Biophys.* 301:41–52.
3. Roher, A. E., J. D. Lowenson, …, M. J. Ball. 1993. β-Amyloid-(1-42) is a major component of cerebrovascular amyloid deposits: implications for the pathology of Alzheimer disease. *Proc. Natl. Acad. Sci. USA.* 90:10836–10840.
4. Lambert, M. P., A. K. Barlow, …, W. L. Klein. 1998. Diffusible, nonfibrillar ligands derived from Aβ1-42 are potent central nervous system neurotoxins. *Proc. Natl. Acad. Sci. USA.* 95:6448–6453.
5. Ferreira, S. T., and W. L. Klein. 2011. The Aβ oligomer hypothesis for synapse failure and memory loss in Alzheimer's disease. *Neurobiol. Learn. Mem.* 96:529–543.
6. Jung, C. K., K. Keppler, …, J. Herms. 2015. Fibrillar amyloid plaque formation precedes microglial activation. *PLoS One.* 10:e0119768.
7. Komatsu, H., E. Feingold-Link, …, P. H. Axelsen. 2010. Intrinsic linear heterogeneity of amyloid β protein fibrils revealed by higher resolution mass-per-length determinations. *J. Biol. Chem.* 285:41843–41851.
8. Petkova, A. T., R. D. Leapman, …, R. Tycko. 2005. Self-propagating, molecular-level polymorphism in Alzheimer's β-amyloid fibrils. *Science.* 307:262–265.
9. Paravastu, A. K., A. T. Petkova, and R. Tycko. 2006. Polymorphic fibril formation by residues 10–40 of the Alzheimer's β-amyloid peptide. *Biophys. J.* 90:4618–4629.
10. Lara, C., J. Adamcik, …, R. Mezzenga. 2011. General self-assembly mechanism converting hydrolyzed globular proteins into giant multistranded amyloid ribbons. *Biomacromolecules.* 12:1868–1875.
11. Dickson, T. C., and J. C. Vickers. 2001. The morphological phenotype of β-amyloid plaques and associated neuritic changes in Alzheimer's disease. *Neuroscience.* 105:99–107.
12. Laganowsky, A., C. Liu, …, D. Eisenberg. 2012. Atomic view of a toxic amyloid small oligomer. *Science.* 335:1228–1231.
13. Liu, C., M. Zhao, …, D. Eisenberg. 2012. Out-of-register β-sheets suggest a pathway to toxic amyloid aggregates. *Proc. Natl. Acad. Sci. USA.* 109:20913–20918.
14. Urbanc, B., L. Cruz, …, B. T. Hyman. 2002. Neurotoxic effects of thioflavin S-positive amyloid deposits in transgenic mice and Alzheimer's disease. *Proc. Natl. Acad. Sci. USA.* 99:13990–13995.
15. Seilheimer, B., B. Bohrmann, …, H. Döbeli. 1997. The toxicity of the Alzheimer's β-amyloid peptide correlates with a distinct fiber morphology. *J. Struct. Biol.* 119:59–71.
16. Olofsson, A., J. Ostman, and E. Lundgren. 2002. Amyloid: morphology and toxicity. *Clin. Chem. Lab. Med.* 40:1266–1270.
17. vandenAkker, C. C., T. Deckert-Gaudig, …, G. H. Koenderink. 2015. Nanoscale heterogeneity of the molecular structure of individual hIAPP amyloid fibrils revealed with tip-enhanced Raman spectroscopy. *Small.* 11:4131–4139.
18. Morel, B., L. Varela, and F. Conejero-Lara. 2010. The thermodynamic stability of amyloid fibrils studied by differential scanning calorimetry. *J. Phys. Chem. B.* 114:4010–4019.
19. Narimoto, T., K. Sakurai, …, Y. Goto. 2004. Conformational stability of amyloid fibrils of β_2-microglobulin probed by guanidine-hydrochloride-induced unfolding. *FEBS Lett.* 576:313–319.
20. Baldwin, A. J., T. P. Knowles, …, C. M. Dobson. 2011. Metastability of native proteins and the phenomenon of amyloid formation. *J. Am. Chem. Soc.* 133:14160–14163.
21. Yoshimura, Y., Y. Lin, …, Y. Goto. 2012. Distinguishing crystal-like amyloid fibrils and glass-like amorphous aggregates from their kinetics of formation. *Proc. Natl. Acad. Sci. USA.* 109:14446–14451.
22. Garai, K., and C. Frieden. 2013. Quantitative analysis of the time course of Aβ oligomerization and subsequent growth steps using

tetramethylrhodamine-labeled Aβ. *Proc. Natl. Acad. Sci. USA.* 110:3321–3326.

23. Garai, K., and C. Frieden. 2010. The association−dissociation behavior of the ApoE proteins: kinetic and equilibrium studies. *Biochemistry.* 49:9533–9541.
24. Gendron, P. O., F. Avaltroni, and K. J. Wilkinson. 2008. Diffusion coefficients of several rhodamine derivatives as determined by pulsed field gradient-nuclear magnetic resonance and fluorescence correlation spectroscopy. *J. Fluoresc.* 18:1093–1101.
25. Garai, K., P. B. Verghese, …, C. Frieden. 2014. The binding of apolipoprotein E to oligomers and fibrils of amyloid-β alters the kinetics of amyloid aggregation. *Biochemistry.* 53:6323–6331.
26. Erijman, L., and G. Weber. 1991. Oligomeric protein associations: transition from stochastic to deterministic equilibrium. *Biochemistry.* 30:1595–1599.
27. Ma, J., H. Komatsu, …, P. H. Axelsen. 2013. Intrinsic structural heterogeneity and long-term maturation of amyloid β peptide fibrils. *ACS Chem. Neurosci.* 4:1236–1243.
28. Calamai, M., C. Canale, …, C. M. Dobson. 2005. Reversal of protein aggregation provides evidence for multiple aggregated states. *J. Mol. Biol.* 346:603–616.
29. Paravastu, A. K., R. D. Leapman, …, R. Tycko. 2008. Molecular structural basis for polymorphism in Alzheimer's β-amyloid fibrils. *Proc. Natl. Acad. Sci. USA.* 105:18349–18354.
30. Tipping, K. W., P. van Oosten-Hawle, …, S. E. Radford. 2015. Amyloid fibres: inert end-stage aggregates or key players in disease? *Trends Biochem. Sci.* 40:719–727.
31. Christensen, D. Z., S. L. Kraus, …, T. A. Bayer. 2008. Transient intraneuronal Aβ rather than extracellular plaque pathology correlates with neuron loss in the frontal cortex of APP/PS1KI mice. *Acta Neuropathol.* 116:647–655.
32. Koffie, R. M., M. Meyer-Luehmann, …, T. L. Spires-Jones. 2009. Oligomeric amyloid β associates with postsynaptic densities and correlates with excitatory synapse loss near senile plaques. *Proc. Natl. Acad. Sci. USA.* 106:4012–4017.
33. Milanesi, L., T. Sheynis, …, H. R. Saibil. 2012. Direct three-dimensional visualization of membrane disruption by amyloid fibrils. *Proc. Natl. Acad. Sci. USA.* 109:20455–20460.
34. Cohen, S. I. A., S. Linse, …, T. P. J. Knowles. 2013. Proliferation of amyloid-β42 aggregates occurs through a secondary nucleation mechanism. *Proc. Natl. Acad. Sci. USA.* 110:9758–9763.
35. Xue, W. F., S. W. Homans, and S. E. Radford. 2008. Systematic analysis of nucleation-dependent polymerization reveals new insights into the mechanism of amyloid self-assembly. *Proc. Natl. Acad. Sci. USA.* 105:8926–8931.
36. Nussbaum-Krammer, C. I., K. W. Park, …, R. I. Morimoto. 2013. Spreading of a prion domain from cell-to-cell by vesicular transport in *Caenorhabditis elegans*. *PLoS Genet.* 9:e1003351.
37. Jaunmuktane, Z., S. Mead, …, S. Brandner. 2015. Evidence for human transmission of amyloid-β pathology and cerebral amyloid angiopathy. *Nature.* 525:247–250.
38. Peelaerts, W., L. Bousset, …, V. Baekelandt. 2015. α-Synuclein strains cause distinct synucleinopathies after local and systemic administration. *Nature.* 522:340–344.
39. Safar, J., H. Wille, …, S. B. Prusiner. 1998. Eight prion strains have PrP(Sc) molecules with different conformations. *Nat. Med.* 4:1157–1165.
40. Cummings, J., T. Morstorf, and G. Lee. 2016. Alzheimer's drug-development pipeline: 2016. *Alzheimers Dement. (N. Y.).* 2:222–232.
41. Sevigny, J., P. Chiao, …, A. Sandrock. 2016. The antibody aducanumab reduces Aβ plaques in Alzheimer's disease. *Nature.* 537:50–56.
42. Nie, Q., X. G. Du, and M. Y. Geng. 2011. Small molecule inhibitors of amyloid β peptide aggregation as a potential therapeutic strategy for Alzheimer's disease. *Acta Pharmacol. Sin.* 32:545–551.
43. Rauth, S., D. Hinz, …, A. Skerra. 2016. High-affinity anticalins with aggregation-blocking activity directed against the Alzheimer β-amyloid peptide. *Biochem. J.* 473:1563–1578.
44. Han, X., J. Park, …, R. M. Leblanc. 2017. A resorcinarene for inhibition of Aβ fibrillation. *Chem. Sci. (Camb.).* 8:2003–2009.
45. Wang, Q., X. Yu, …, J. Zheng. 2013. Tanshinones inhibit amyloid aggregation by amyloid-β peptide, disaggregate amyloid fibrils, and protect cultured cells. *ACS Chem. Neurosci.* 4:1004–1015.
46. Noor, H., P. Cao, and D. P. Raleigh. 2012. Morin hydrate inhibits amyloid formation by islet amyloid polypeptide and disaggregates amyloid fibers. *Protein Sci.* 21:373–382.
47. Knowles, T. P., A. W. Fitzpatrick, …, M. E. Welland. 2007. Role of intermolecular forces in defining material properties of protein nanofibrils. *Science.* 318:1900–1903.
48. Knowles, T. P., and M. J. Buehler. 2011. Nanomechanics of functional and pathological amyloid materials. *Nat. Nanotechnol.* 6:469–479.
49. Crick, S. L., K. M. Ruff, …, R. V. Pappu. 2013. Unmasking the roles of N- and C-terminal flanking sequences from exon 1 of huntingtin as modulators of polyglutamine aggregation. *Proc. Natl. Acad. Sci. USA.* 110:20075–20080.
50. Cellmer, T., R. Douma, …, H. Blanch. 2007. Kinetic studies of protein L aggregation and disaggregation. *Biophys. Chem.* 125:350–359.
51. Gorman, P. M., C. M. Yip, …, A. Chakrabartty. 2003. Alternate aggregation pathways of the Alzheimer β-amyloid peptide: Aβ association kinetics at endosomal pH. *J. Mol. Biol.* 325:743–757.
52. Carulla, N., M. Zhou, …, C. M. Dobson. 2009. Experimental characterization of disordered and ordered aggregates populated during the process of amyloid fibril formation. *Proc. Natl. Acad. Sci. USA.* 106:7828–7833.
53. Shih, Y. C., J. M. Prausnitz, and H. W. Blanch. 1992. Some characteristics of protein precipitation by salts. *Biotechnol. Bioeng.* 40:1155–1164.
54. Silva, J. L., M. Villas-Boas, …, N. C. Meirelles. 1989. Anomalous pressure dissociation of large protein aggregates. Lack of concentration dependence and irreversibility at extreme degrees of dissociation of extracellular hemoglobin. *J. Biol. Chem.* 264:15863–15868.
55. Silva, J. L., and G. Weber. 1988. Pressure-induced dissociation of brome mosaic virus. *J. Mol. Biol.* 199:149–159.
56. Botelho, M. G., A. W. Rietveld, and S. T. Ferreira. 2006. Long-lived conformational isomerism of protein dimers: the role of the free energy of subunit association. *Biophys. J.* 91:2826–2832.
57. Liu, J., I. Costantino, …, L. Makowski. 2016. Amyloid structure exhibits polymorphism on multiple length scales in human brain tissue. *Sci. Rep.* 6:33079.
58. Rogovina, L. Z., and G. L. Slonimskii. 1974. Formation, structure, and properties of polymer gels. *Russ. Chem. Rev.* 43:503–523.
59. Mercadé-Prieto, R., R. J. Falconer, …, D. I. Wilson. 2006. Effect of gel structure on the dissolution of heat-induced β-lactoglobulin gels in alkali. *J. Agric. Food Chem.* 54:5437–5444.
60. Benz, M., W. B. Euler, and O. J. Gregory. 2001. The influence of preparation conditions on the surface morphology of poly(vinylidene fluoride) films. *Langmuir.* 17:239–243.
61. Ouano, A. C., and J. A. Carothers. 1980. Dissolution dynamics of some polymers—solvent polymer boundaries. *Polym. Eng. Sci.* 20:160–166.
62. Peppas, N. A., J. C. Wu, and E. D. Vonmeerwall. 1994. Mathematical-modeling and experimental characterization of polymer dissolution. *Macromolecules.* 27:5626–5638.
63. Flory, P. J. 1953. Principles of Polymer Chemistry. Cornell University Press, Ithaca, NY.
64. Aghanouri, A., and G. Sun. 2015. Hansen solubility parameters as a useful tool in searching for solvents for soy proteins. *RSC Advances.* 5:1890–1892.